UV-A to UV-B electroluminescence of core-shell GaN/AlGaN wire heterostructures

Vincent Grenier, Sylvain Finot, Lucie Valera, Joël Eymery, Gwénolé Jacopin, Christophe Durand

UV-A to UV-B electroluminescence of core-shell GaN/AlGaN wire heterostructures

Vincent Grenier[1], Sylvain Finot[2], Lucie Valera[1], Joël Eymery[3], Gwénolé Jacopin[2], Christophe Durand[1,a)]

[1] *Univ. Grenoble Alpes, CEA, IRIG, PHELIQS, NPSC, 38000 Grenoble, France*

[2] *Univ. Grenoble Alpes, CNRS, Grenoble INP, Institut Néel, 38000 Grenoble, France*

[3] *Univ. Grenoble Alpes, CEA, IRIG, MEM, NRS, 38000 Grenoble, France*

a) Author to whom correspondence should be addressed*: christophe.durand@cea.fr*

Keywords: GaN/AlGaN MQWs, LED, core-shell microwires, MOVPE

ABSTRACT :

Core-shell GaN/AlGaN multiple quantum wells (MQWs) embedded in p-n junction are integrated on the upper part of GaN microwires grown by silane-assisted metal organic vapor phase epitaxy. Dispersed wires are then contacted by electron beam induced deposition for the fabrication of single wire UV-LED devices. Rectifying diode-like behavior is firstly demonstrated for both n-GaN/p-GaN and n-GaN/p-AlGaN junctions without MQW active region. A weak leakage current in the GaN/AlGaN core-shell heterostructure is attributed to an additional conduction path along wire sidewalls. Electroluminescence at 340 nm in UV-A is demonstrated using GaN (2.6 nm)/$Al_{0.3}Ga_{0.7}N$ (3 nm) heterostructure embedded in GaN/$Al_{0.3}Ga_{0.7}N$ p-n junction. This value is even decreased to 310 nm by reducing well thickness to 0.9 nm and increasing the Al-content of barriers (up to 60%) integrated in GaN/$Al_{0.3}Ga_{0.7}N$ p-n junction. This work demonstrates UV-B emission based on single wire core-shell UV-LED.

Light emitting diodes (LEDs) based on III-N semiconductors are excellent solutions for the increasing demand of Hg-free ultraviolet (UV) sources. The wavelength of UV-LEDs can be controlled depending on the targeted applications. For instance, the UV-A (400-315 nm) and UV-B (315-280 nm) are applied for curing, sensing, plant lighting and medical treatments, while the UV-C (280-200 nm) is mainly dedicated for bactericidal and virucidal applications. Despite more than 20 years of research on planar UV-LEDs leading to significant optimizations, external quantum efficiency (EQE) remains relatively low in comparison to visible LEDs (below 20% for UV-C[1] vs above 80% for blue emission). This low efficiency is related to extended and point defects, poor light extraction and the issue of Al-rich AlGaN p-doping.[2] The use of nano/microwires has recently emerged to go further in the UV-LED development, due to the drastic reduction of extended defects[3,4] and also a more efficient p-doping for UV-C emission.[5,6] With the wire approach, the active region in core-shell geometry grown on *m*-plane surfaces offers additional advantages, such as the absence of the quantum confined Stark effect, the significant increase of emitting area and the possibility to make micro-sized UV-sources[7] or flexible LEDs/photodetectors.[8–10]

Core-shell UV emission has been already demonstrated by several multiple quantum well (MQW) heterostructures: GaN/AlN,[11] GaN/InAlN,[12,13] GaN/AlGaN,[14,15] AlGaN/AlGaN[16,17] and AlGaN/AlN.[18] However, core-shell electroluminescence (EL) is yet rarely reported and only limited to the UV-A range. Indeed, 365 nm EL was obtained for a core-shell n-i-p $Al_{0.1}Ga_{0.9}N$ heterostructure without embedded MQWs,[19] and 318 nm EL for core-shell AlGaN MQWs in a p-n AlGaN junction.[17] In this context, one of the main issues for core-shell heterostructures is to address electroluminescence beyond the UV-A.

This work targets UV-B electroluminescence with GaN microwires using core-shell GaN/AlGaN MQWs embedded in p-n junction. We first study GaN and AlGaN core-shell p-n junctions to understand the electrical properties of single wire UV-LEDs. Two types of core-shell LED structures are then designed to demonstrate EL both in UV-A and UV-B ranges. As the UV emission wavelength can be directly tuned by the QW thickness in core-shell GaN/AlGaN MQW system,[14] 2.6 nm-thick GaN QWs are accordingly chosen for UV-A, whereas thinner 0.9 nm-thick QWs are preferred to get UV-B.

Core-shell microwires are grown by metal-organic vapor phase epitaxy (MOVPE) on nitridated c-sapphire substrates to promote the N-polarity growth[20] using a silane-assisted method.[21] The silane flow (set to 200 nmol/min) induces a very high n-doping level in the wire bottom part (~10^{20} at./cm^3,[22] called "n^{++}-part") and the formation of the SiN_x passivation layer on the *m*-plane sidewalls enhancing the vertical growth. At the second step of the growth, the silane is switched off and its residue leads to an unintentional n-doping level in the wire upper part (~10^{19} at./cm^3,[23] called "n^{+}-part"). The shell structure grown at 920°C begin with an unintentional n-doped GaN spacer (~50 nm at 150 mbar), which covers the n^{+}-part thanks to the absence of the passivation layer. This GaN spacer allows burying the surface defects of the wire top part induced by the formation of an ultrathin $SiGa_xN_y$ residual layer.[24] The n-doped shell of the LED structure grown at 100 mbar is composed of a 20 nm-thick n-doped $Al_xGa_{1-x}N$ layer with a linear gradient (x = 0-30%) followed by a 10 nm-thick n-$Al_{0.3}Ga_{0.7}N$ layer. Precursors and gas flows are respectively 0-3.65, 3.6, 66 900, 0.012 µmol.min^{-1} for trimethyl-Aluminium (TMAl), triethyl-Gallium (TEGa), NH_3 and silane flows. Then, the active region either UV-A or UV-B is grown, named "Structure A" and "Structure B", respectively. For both structures, the active region is ended by a ~10 nm-thick p-$Al_{0.3}Ga_{0.7}N$ layer is then grown with a Cp_2Mg precursors flux set to 0.3 µmol.min^{-1}, followed by a ~50 nm-thick p-GaN layer grown

using 178 mmol.min^{-1} of NH_3, 45 and 0.7 µmol.min^{-1} for TMGa and Cp_2Mg precursors. The shell is ended by a thin p^+-doped GaN layer (34 and 0.8 µmol.min^{-1} for TMGa and Cp_2Mg). The Mg-dopant activation is achieved by a thermal annealing at 700 °C for 20 min under nitrogen. The grown core-shell wires have a typical diameter of about 1 µm at the base for a total length of 20-25 µm (density of 10^7 wires/cm^2).

For the sake of simplicity, we decided here to electrically contact the wire with a rapid technique without lithography, called EBID (Electron Beam Induced Deposition), which is particularly well adapted to this study due to the ease of mechanically dispersing the wires on any substrate. In addition, this core-shell geometry allows a direct access to the p-GaN shell at the upper part of the wires and to the n^{++}-GaN core at the bottom part. Byeong-Seon An *et al.* reports on the relatively high percentage of carbon and oxygen in EBID deposited materials (attributed to the insufficient decomposition of the W precursor ($W(CO)_6$)) that induces more resistive contacts.[25] High-energy IBID (Ion Beam Induced Deposition) is an alternative for efficient $W(CO)_6$ decomposition, increasing the contact conductivity. However, this technique has been ruled out considering the damage caused by the Ga^+ ion on the structure, and EBID has been preferred. As shown in the SEM image of Figure I, microwires are directly dispersed on a silicon substrate coated with an insulating SiO_2 layer, on which Ni/Au metal patterns (in yellow) are deposited by a lithography process. Figure I(a,b) illustrates the possibility to move the selected wire (green) between two Ni/Au contacts (yellow) using a micromanipulator. Once the wire is in place, an injector is inserted near the sample and releases the organo-metallic tungsten precursors $W(CO)_6$. To contact the core-shell wires, the electron beam is set to deposition conditions (3 kV, 17 nA) and the observation window is reduced to decompose the precursor only in the area corresponding to the two zones delimited by red dashed rectangles in Figure I(c), i.e., p-GaN shell and n^{++}-GaN wire base, respectively.

Usually, the Al-rich active part of deep UV-LED devices is embedded in an AlGaN p-n junction. In this work, the core-shell active layer is buried under a Mg p-doped layer, as it has been already demonstrated in microwire LEDs for visible emission.[26] However, extending the Mg doping procedure to AlGaN alloys is still challenging, and only few studies investigated it on *m*-plane surfaces.[19,27] To study the electrical characteristics of AlGaN p-n junction in core-shell geometry, two first structures were grown without active part as shown in Figure 2(a): first, a core-shell structure with only a GaN p-n junction (named structure 1), and second, a structure with an additional embedded $Al_{0.3}Ga_{0.7}N$ p-n junction (named structure 2). As shown in Figure 2(b), I-V measurements are performed on several wires with core-shell structure 1 (red curves) and 2 (green curves), contacted with the EBID method. For both structures, a clear rectifying profile is observed with standard diode-like behavior. We measure higher turn-on voltages for the $Al_{0.3}Ga_{0.7}N$ p-n junction due to the larger band gap energy, and also a large threshold value dispersion (+2 to +5 V) probably related to the low quality and reproducibility of the p^+-GaN/W EBID contacts.[28] Structure 1 exhibits an average current of 80 µA at 5.8 ±1 V, while the same current level is reached at 9.1 ±0.9 V for Structure 2. The inset of Figure 2(b) showing I-V data in logarithmic scale demonstrates that the leakage currents of the GaN junction (structure 1) are very low (below the detection limit ≈ 10^{-6} µA), whereas for the $Al_{0.3}Ga_{0.7}N$ p-n junction (structure 2), higher leakage currents are measured in the order of 10^{-1}-10^{-3} µA. We suspect that these parasitic currents come from the activation of an additional conduction path through the wire sidewalls (see the schematic of Figure 2(c)). Thus, as shown in the SEM images of Figure 2(c), the Structure 1 without Al shows the p-GaN shell only on the wire upper part (bright contrast). On the contrary, for Structure 2 involving AlGaN growth, the p-GaN shell grows on both parts (n^{++}- and n^+-GaN) of the wires. Indeed, we observe that the radial growth

of the Al-based layers is not selective and buries the SiN_x passivation layer on the wire bottom part, as already reported.[14] We can also note that the p-GaN thickness at the wire bottom part decreases as we approach its base (see the contrast variation), and it may be possible to circumvent this problem by growing longer GaN wires. These first electrical characterizations of the core-shell structures demonstrate the suitability of the core-shell GaN/GaN and GaN/AlGaN p-n junctions.

The active region of "Structure A" detailed in Figure 3(a) is designed for UV-A emission by incorporating five periods of 2.6 nm-thick GaN QW embedded in 3 nm-thick $Al_{0.3}Ga_{0.7}N$ barrier. This active MQW region is integrated in a p-n junction corresponding to the following core-shell heterostructure n-GaN/n-$Al_{0.3}Ga_{0.7}N$/MQWs/p-$Al_{0.3}Ga_{0.7}N$/p-GaN junction. After contacting several microwire devices by EBID, I-V measurements are performed at room temperature. It is shown from the measurements in Figure 3(b) that the addition of the GaN/ $Al_{0.3}Ga_{0.7}N$ quantum wells does not significantly affect the electrical properties of the diode. Indeed, a rectifying behavior similar to the GaN/AlGaN p-n junction without heterostructure is measured with a current of 80 µA near 9 V. The inset shows the log scale curves exhibiting leakage currents in the same range of magnitude as for the GaN/AlGaN p-n junction (10^{-2} - 10^{-5} µA at -5 V). Figure 3(c) shows an SEM image of a typical wire with core-shell structure A with its EBIC (Electron Beam Induced Current) signal mapping. This measurement is obtained by placing tips on the Ni/Au contacts connected to the n- and p-sides of the wire without applied voltage bias and by injecting electrons locally via the SEM electron beam scanning operating at 2 kV. Note that in our geometry the excitation is parallel to the p-n junction[29] and not perpendicular as it is usually the case to extract minority carrier diffusion length.[30] Therefore, minority hole carriers play a role in signal generation, but the EBIC mapping also reflects transport properties of majority electron carriers.[29] As observed in Figure 3(c), the EBIC signal

only comes from the wire upper part. It evidences the signature of the core-shell p-n junction located only on the wire upper part, in agreement with previous measurements on core-shell InGaN/GaN MQW wires.[23,29] The absence of EBIC signal underneath the p-GaN contact can be directly attributed to a shadowing of the electron beam by the tungsten deposit.[29]

Electroluminescence (EL) measurements were carried out by applying a pulsed voltage at 10 kHz frequency and 1% duty cycle to prevent the damage of wire devices by Joule heating. The EL measurements shown in Figure 3(d) were performed by applying a peak voltage ranging from 12 to 18 V. The location of EL emission is expected to come from the core-shell structure in accordance with EBIC signal and core-shell CL emission of UV MQWs (no emission is observed on N-polar c-top surface).[14] Three main contributions are identified: (i) the yellow band (YB) emission at around 2.25 eV related to deep defects in GaN,[31] (ii) an asymmetric contribution at 3.35 eV called violet band (VB), (iii) the contribution at higher energy coming from the GaN MQWs with a UV-A emission centered at 3.65 eV (340 nm) having a FWHM of ≈ 150 meV. From the evolution of the EL intensity as a function of the applied voltage, we observe that the QW emission intensity significantly increases at high voltage till to dominate the VB contribution. The room temperature CL spectrum of the same wire is shown in inset of Figure 3(d). In contrast with EL measurements, the main CL emission at 2 kV excitation comes from the QW contribution localized at the same position than EL emission at 3.65 eV (340 nm) and the two peaks observed at 3.43 eV (362 nm) and 3.35 eV (370 nm) attributed respectively to the near band edge of n-doped GaN and the VB emission are much weaker. This VB emission becomes dominant in CL spectra for low acceleration voltage (below 1 kV). We suspect that the origin of the VB emission comes from the external shell layers and most probably from the donor/acceptor pairs (DAPs) contribution in the p-GaN.[32] The intense VB emission, as well as the high voltages required for the QW emission, could be the sign of a

poor hole injection in the active region (with parasitic conduction paths) combined with a poor electrical injection at the metallic contact level. Moreover, a phenomenon of electron overflow is suspected: the absence of EBL can involve a significant radiative recombination on the p-side shell. The hole injection issue is expected to be amplified in the case of a structure designed for deeper UV emission, including Al-rich layers.

The active region of "Structure B" detailed in Figure 4(a) is now designed for UV-B emission consisting in five periods of thinner GaN QW estimated at 0.9 nm embedded in 3 nm-thick $Al_{0.6}Ga_{0.4}N$ barrier (QW growth time three times shorter with doubled TMAl flow in comparison of the structure A). This UV-B active region is integrated in a p-n junction corresponding to the following core-shell heterostructure n-GaN/n-$Al_{0.3}Ga_{0.7}N$/MQWs/20 nm-thick graded p-$Al_xGa_{1-x}N$ (x=60-30%)/p-$Al_{0.3}Ga_{0.7}N$/p-GaN junction. To ensure quantum confinement, the GaN layers are separated by 3 nm $Al_{0.6}Ga_{0.4}N$ barriers instead of $Al_{0.3}Ga_{0.7}N$ used for the UV-A structure. It is important to note that for such ultrathin GaN layers grown on *m*-plane $Al_{0.6}Ga_{0.4}N$, a quantum dot like regime is usually observed with strong confinement and localization.[14,15] To address the hole injection issue, we incorporated a p-doped linear AlGaN gradient with 60-30 % Al composition between the active part and the p-$Al_{0.3}Ga_{0.7}N$ layer, as already used in UV planar structures.[33,34]

Figure 4(b) shows the I-V measurements performed on several UV-B core-shell wires. As expected, UV-B devices do not show as good rectifying behavior as the UV-A ones. The forward current of 10^{-1} -10^{-2} µA measured at 10 V for UV-B devices is 3-4 orders of magnitude lower than in UV-A devices. The log scale curves shown in inset exhibit leakage currents in the same order of magnitude as for the core-shell structures 2 and A, i.e., 10^{-2} -10^{-5} µA at -5 V. Those values indicate that the leakage currents are not dependent on the quantity of Al in the shell, which is in agreement with the assumption of a parallel conduction path through the p-

GaN shell presented in Figure 2(c). Figure 4(c) shows a SEM image of an EBID contacted UV-B core-shell wire and the corresponding EBIC signal mapping. As for the UV-A structure, the EBIC signal is only measured on the n^+-GaN part of the wire, where is situated the GaN/AlGaN p-n junction and active part. In contrast to the UV-A structure, dark lines are observed on the EBIC mapping, revealing the presence of several cracks on the wire. This type of defects already studied in the literature results from the elastic relaxation of the Al-rich shells and affects the CL and PL emissions of the MQWs.[15] This observation also confirms the detrimental effect of cracks on the electroluminescence of these devices, but does not increase the leakage currents with respect to the crack-free AlGaN p-n junction and UV-A structures, see Figure 2(b) and 3(b). EL is obtained in the targeted UV-B range as shown in Figure 4(d) despite low forward currents and multiple cracks. Similarly to the UV-A sample, the EL emission comes from core-shell structures considering the EBIC and CL mappings exhibiting core-shell emissions (no emission from N-polar c-flat top surface).[14] By applying a pulsed voltage of 7 to 14 V, the three contributions previously discussed are found: the YB and VB bands, the UV-B emission centered at 4 eV (310 nm) coming from confined charge carriers in GaN. The MQW emission is clearly pronounced with respect to the VB band at 14V in comparison of the device A for the same voltage, proving the effective hole injection despite the addition of the p-AlGaN gradient. This device demonstrates an UV-B electroluminescence at 310 nm with core-shell GaN/$Al_{0.6}Ga_{0.4}N$ heterostructure.

Figure 5 makes a comparison of EL emissions from 3 different core-shell heterostructures: the pure GaN p-n junction without MQW (structure 1), the UV-A LED (structure A) and the UV-B LED (structure B). Interestingly, we do observe the VB emission ranging 3.2-3.4 eV also for the structure 1 with only GaN p-n junction. This observation confirms that the VB emission comes from the GaN related to the DAP contribution of p-doped GaN[32] for all three samples. In

addition, a weak UV emission of GaN is visible in the tail of VB emission near 3.4 eV (365 nm). For LED structure based on MQWs, the UV emission move at 3.7 eV for the UV-A structure and up to 4 eV for the UV-B structure. A broadening of the MQW UV emission is observed, especially on UV-B emission (full width at half maximum (FWHM) equal to 150 eV and 250 meV for UV-A and UV-B emission), which is perfectly consistent with the increasing width of UV emission by decreasing GaN MQW thickness, as measured by photoluminescence on the same core-shell GaN/AlGaN MQW system.[14] This broadening is mainly related to the wall-to-wall variation of GaN QW thickness (possible variation up to 40-50%) for the UV-A emission, whereas the dot-like emission is more observed on the UV-B emission that contributes to broaden the emission over a larger range due to local QW thickness variations.[14]

In conclusion, the electrical characterization and electroluminescence of core-shell GaN/AlGaN heterostructures grown on *m*-plane sidewalls of GaN wires have been performed on single wire devices contacted with the EBID technique. We demonstrated with core-shell GaN/GaN and GaN/AlGaN p-n junctions (and without the addition of MQWs) a rectifying diode behavior. In addition, an increase of leakage currents is measured when the growth involves AlGaN-based shells, indicating the presence of a conduction path along wire sidewalls through the p-GaN shell grown on AlGaN under-shell. A first device is developed for UV-A emission with 2.6 nm-thick GaN wells. Electroluminescence at 340 nm is demonstrated and EBIC mapping confirmed the core-shell p-n junction located at the wire upper part (Si n^+-doped GaN). EL measurements also revealed a strong DAP signal coming from the Mg p-doped GaN external shell. This contribution could be reduced by improving the hole injection in the active region and by adding an electron blocking layer to limit electron overflow. A second device designed for UV-B emission is achieved by reducing the QW thickness to 0.9 nm and increasing the Al composition in the barriers up to 60 %. Such wires exhibit an electroluminescence at

310 nm allowing to reach the UV-B emission from core-shell wire-based UV-LEDs. This work represents a milestone in the development of core-shell wires for deep UV applications.

Author Contributions

V.G. performed the wire growth process and took an active part in the writing of this manuscript with support from the supervisors C.D. and J.E. who designed the study. S.F and G.J performed the CL, EL and EBIC measurements. Lucie Valera performed the SEM observations. The wire contact by EBID and I-V measurements were performed by V.G. All authors contributed to the discussions and have given approval to the final version of the manuscript.

Notes

The authors declare no competing financial interest.

Aknowledgments

This work was financially supported by the program Initiatives de Recherche Stratégiques (IRS) of IDEX Université Grenoble Alpes (15-IDEX-0002). The authors thank J. Dussaud for his work on the MOVPE setup.

Figure captions

Figure 1: a,b) SEM images of microwire (green) displaced on Ni/Au contacts (yellow) using a micromanipulator (blue). c) SEM image of tungsten deposition (red rectangle) by EBID (3 kV, 17 nA) to perform n and p contacts of a core-shell GaN microwire (green).

Figure 2: (a) Schematic of core-shell structures with GaN single p-n junction (structure 1) and GaN/AlGaN p-n junction (structure 2). b) Room temperature I-V curves of structures 1 (red) and 2 (green). The inset shows the I-V curves in logarithmic scale. c) Schematics and SEM images of core-shell wires grown in 600/700 s for the n^{++}/n^{+}-GaN parts: (left) GaN p-n junction and (right) GaN/AlGaN p-n junction. In the SEM images, the p-GaN layer that finishes the shell growth of both structures appears with a bright contrast. The schematics show a single core-shell wire contacted with tungsten. In the case where the growth involves AlGaN layer(s) (right), the leakage and forward current paths are represented by dotted lines.

Figure 3: a) Schematic of the core-shell structure for UV-A emission with 5x GaN (2.6 nm)/ $Al_{0.3}Ga_{0.7}N$ (3 nm) quantum wells integrated in a GaN/ $Al_{0.3}Ga_{0.7}N$ p-n junction. b) Room temperature I-V curves on several single wires with core-shell structure A, connected using EBID method. c) SEM image and EBIC mapping of a typical A-type core-shell wire. d) Electroluminescence spectra on a single structure A wire obtained at room temperature with a pulsed voltage whose peak varies from 12 to 18 V. The inset shows the CL spectrum of the same wire, acquired with a 2 kV acceleration voltage.

Figure 4: a) Schematic of the core-shell structure for UV-B emission with 5x GaN (0.9 nm)/ $Al_{0.6}Ga_{0.4}N$ (3 nm) quantum dots integrated in a GaN/ $Al_{0.3}Ga_{0.7}N$ p-n junction. b) Room temperature I-V curves on several single wires with core-shell structure B, connected using EBID method. c) SEM image and EBIC mapping of a typical B-type core-shell wire. d) Electroluminescence spectra on a single structure B wire obtained at room with a pulsed voltage whose peak varies from 7 to 14 V.

Figure 5: Comparison of EL spectra measured on contacted single wires from 3 core-shell heterostructures: a) pure GaN p-n junction (structure 1), b) UV-A LED (structure A) and c) UV-B LED (structure B).

Bibliography

[1] T. Takano, T. Mino, J. Sakai, N. Noguchi, K. Tsubaki, and H. Hirayama, Appl. Phys. Express **10**, 031002 (2017).

[2] M. Kneissl, T.Y. Seong, J. Han, and H. Amano, Nat. Photonics **13**, 233 (2019).

[3] M. Shatalov, W. Sun, A. Lunev, X. Hu, A. Dobrinsky, Y. Bilenko, J. Yang, M. Shur, R. Gaska, C.G. Moe, G.A. Garrett, and M. Wraback, Appl. Phys. Express **5**, 082101 (2012).

[4] K. Kishino and S. Ishizawa, Nanotechnology **26**, 225602 (2015).

[5] A.M. Siladie, G. Jacopin, A. Cros, N. Garro, E. Robin, D. Caliste, P. Pochet, F. Donatini, J. Pernot, and B. Daudin, Nano Lett. **19**, 8357 (2019).

[6] N.H. Tran, B.H. Le, S. Zhao, and Z. Mi, Appl. Phys. Lett. **110**, 032102 (2017).

[7] H.S. Wasisto, J.D. Prades, J. Gülink, and A. Waag, Appl. Phys. Rev. **6**, 041315 (2019).

[8] H. Zhang, X. Dai, N. Guan, A. Messanvi, V. Neplokh, V. Piazza, M. Vallo, C. Bougerol, F.H. Julien, A. Babichev, N. Cavassilas, M. Bescond, F. MICHELINI, M. Foldyna, E. Gautier, C. Durand, J. Eymery, and M. Tchernycheva, ACS Appl. Mater. Interfaces **8**, 26198 (n.d.).

[9] N. Guan, X. Dai, A. Messanvi, H. Zhang, J. Yan, E. Gautier, C. Bougerol, F.H. Julien, C. Durand, J. Eymery, and M. Tchernycheva, ACS Photonics **3**, 597 (2016).

[10] X. Dai, A. Messanvi, H. Zhang, C. Durand, J. Eymery, C. Bougerol, F.H. Julien, and M. Tchernycheva, Nano Lett. **15**, 6958 (2015).

[11] F. Qian, M. Brewster, S.K. Lim, Y. Ling, C. Greene, O. Laboutin, J.W. Johnson, S. Gradecak, Y. Cao, and Y. Li, Nano Lett. **12**, 3344 (2012).

[12] C. Durand, C. Bougerol, J.F. Carlin, G. Rossbach, F. Godel, J. Eymery, P.H. Jouneau, A. Mukhtarova, R. Butté, and N. Grandjean, ACS Photonics **1**, 38 (2014).

[13] C. Durand, J.-F. Carlin, C. Bougerol, B. Gayral, D. Salomon, J.-P. Barnes, J. Eymery, R. Butté,

and N. Grandjean, Nano Lett. **17**, (2017).

[14] V. Grenier, S. Finot, G. Jacopin, C. Bougerol, E. Robin, N. Mollard, B. Gayral, E. Monroy, J. Eymery, and C. Durand, ACS Appl. Mater. Interfaces **12**, 44007 (2020).

[15] V. Grenier, S. Finot, B. Gayral, C. Bougerol, G. Jacopin, J. Eymery, and C. Durand, Cryst. Growth Des. **21**, 6504 (2021).

[16] S. Finot, V. Grenier, V. Zubialevich, C. Bougerol, P. Pampili, J. Eymery, P.J. Parbrook, C. Durand, and G. Jacopin, Appl. Phys. Lett. **117**, 221105 (2020).

[17] Y. Ra, S. Kang, and C. Lee, Adv. Opt. Mater. **6**, 1701391 (2018).

[18] P.M. Coulon, G. Kusch, R.W. Martin, and P.A. Shields, ACS Appl. Mater. Interfaces **10**, 33441 (2018).

[19] M.D. Brubaker, K.L. Genter, A. Roshko, P.T. Blanchard, B.T. Spann, T.E. Harvey, and K.A. Bertness, Nanotechnology **30**, 234001 (2019).

[20] X.J. Chen, G. Perillat-Merceroz, D. Sam-Giao, C. Durand, and J. Eymery, Appl. Phys. Lett. **97**, 151909 (2010).

[21] R. Koester, J.S. Hwang, C. Durand, D.L.S. Dang, and J. Eymery, Nanotechnology **21**, 015602 (2010).

[22] P. Tchoulfian, F. Donatini, F. Levy, B. Amstatt, P. Ferret, and J. Pernot, Appl. Phys. Lett. **102**, 122116 (2013).

[23] P. Tchoulfian, F. Donatini, F. Levy, A. Dussaigne, P. Ferret, and J. Pernot, Nano Lett. **14**, 3491 (2014).

[24] A. Kapoor, S. Finot, V. Grenier, E. Robin, C. Bougerol, J. Bleuse, G. Jacopin, J. Eymery, and C. Durand, ACS Appl. Mater. Interfaces **12**, 19092 (2020).

[25] B.-S. An, Y. Kwon, J.-S. Oh, Y.-J. Shin, J. Ju, and C.-W. Yang, Appl. Microsc. **49**, (2019).

[26] A. Kapoor, N. Guan, M. VALLO, A. Messanvi, L. Mancini, E. Gautier, C. Bougerol, B. Gayral,

F.H. Julien, F. Vurpillot, L. Rigutti, M. Tchernycheva, J. Eymery, and C. Durand, ACS Photonics **5**, 4330 (2018).

[27] K. Balakrishnan, V. Adivarahan, Q. Fareed, M. Lachab, B. Zhang, and A. Khan, Jpn. J. Appl. Phys. **49**, 0402061 (2010).

[28] I. Hwang, J. Kim, H.S. Choi, H. Choi, J. Lee, K.Y. Kim, J.B. Park, J.C. Lee, J. Ha, J. Oh, J. Shin, and U.I. Chung, IEEE Electron Device Lett. **34**, 202 (2013).

[29] P. Lavenus, a Messanvi, L. Rigutti, a De Luna Bugallo, H. Zhang, F. Bayle, F.H. Julien, J. Eymery, C. Durand, and M. Tchernycheva, Nanotechnology **25**, 255201 (2014).

[30] R. Zhou, M. Yu, D. Tweddle, P. Hamer, D. Chen, B. Hallam, A. Ciesla, P.P. Altermatt, P.R. Wilshaw, and R.S. Bonilla, J. Appl. Phys. **127**, (2020).

[31] R. Koester, J.S. Hwang, C. Durand, D.L.S. Dang, and J. Eymery, Nanotechnology **21**, 015602 (2010).

[32] M.A. Reshchikov, G.C. Yi, and B.W. Wessels, Phys. Rev. B - Condens. Matter Mater. Phys. **59**, 13176 (1999).

[33] J. Yan, J. Wang, P. Cong, L. Sun, N. Liu, Z. Liu, C. Zhao, and J. Li, Phys. Status Solidi Curr. Top. Solid State Phys. **8**, 461 (2011).

[34] Y.K. Kuo, J.Y. Chang, F.M. Chen, Y.H. Shih, and H.T. Chang, IEEE J. Quantum Electron. **52**, (2016).

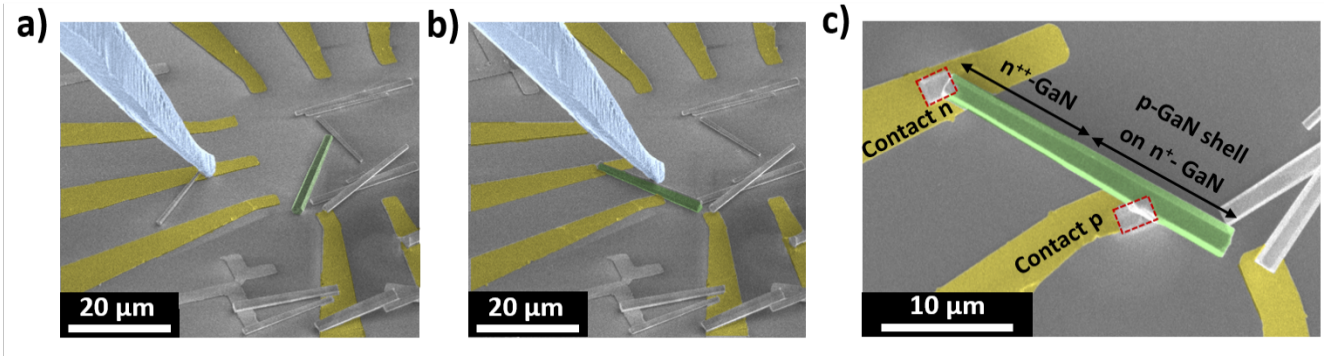
a)
20 µm
b)
20 µm
c)
Contact n
n++-GaN
p-GaN shell
on n+- GaN
Contact p
10 µm

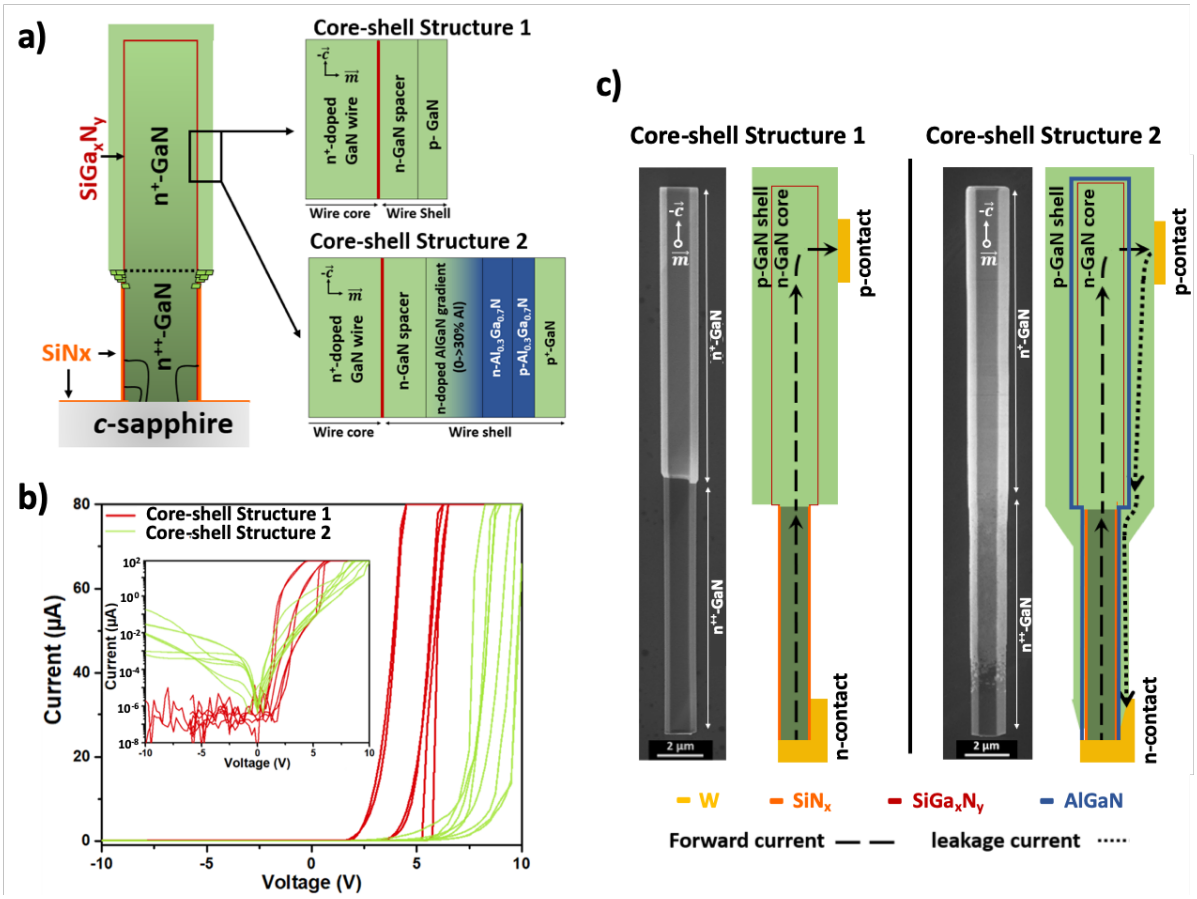
a)
Core-shell Structure 1
Core-shell Structure 2
SiGaxNy
n++-GaN
SiNx
c-sapphire
n+-doped GaN wire
n-GaN spacer
p- GaN
n-doped AlGaN gradient (0->30% Al)
n-Al0.3Ga0.7N
p-Al0.3Ga0.7N
p+-GaN
Wire core
Wire Shell
Wire shell
b)
Core-shell Structure 1
Core-shell Structure 2
Current (μA)
Voltage (V)
c)
Core-shell Structure 1
Core-shell Structure 2
p-GaN shell
n-GaN core
p-contact
n-contact
n+-GaN
n++-GaN
2 μm
W
SiNx
SiGaxNy
AlGaN
Forward current
leakage current

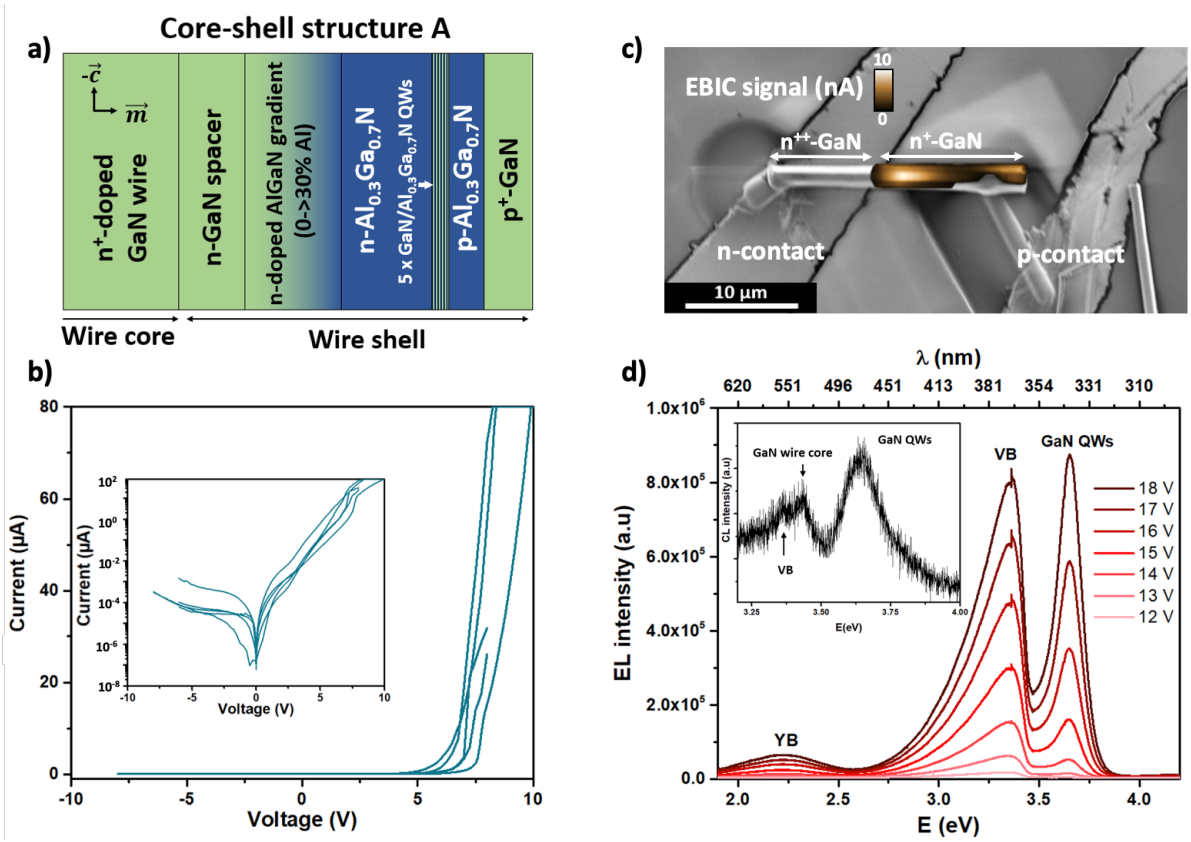
a)
Core-shell structure A
n+-doped GaN wire
n-GaN spacer
n-doped AlGaN gradient (0->30% Al)
n-Al0.3Ga0.7N
5 x GaN/Al0.3Ga0.7N QWs
p-Al0.3Ga0.7N
p+-GaN
Wire core
Wire shell
b)
Current (μA)
Voltage (V)
c)
EBIC signal (nA)
10
0
n++-GaN
n+-GaN
n-contact
p-contact
10 μm
d)
λ (nm)
620 551 496 451 413 381 354 331 310
EL intensity (a.u)
E (eV)
GaN wire core
GaN QWs
VB
YB
CL intensity (a.u)
E(eV)
18 V
17 V
16 V
15 V
14 V
13 V
12 V

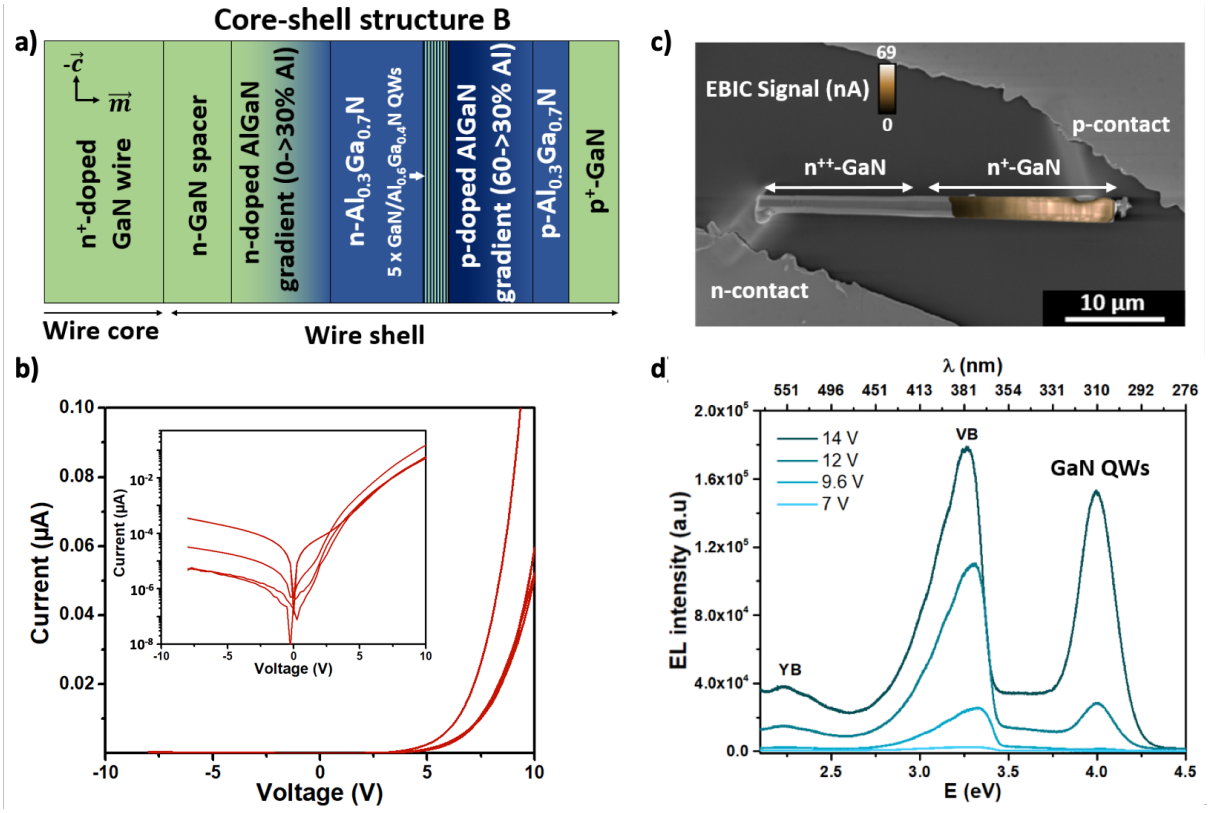
a)
Core-shell structure B
n+-doped GaN wire
n-GaN spacer
n-doped AlGaN gradient (0->30% Al)
n-Al0.3Ga0.7N
5 x GaN/Al0.6Ga0.4N QWs
p-doped AlGaN gradient (60->30% Al)
p-Al0.3Ga0.7N
p+-GaN
Wire core
Wire shell
b)
Current (μA)
Voltage (V)
c)
EBIC Signal (nA)
69
0
p-contact
n++-GaN
n+-GaN
n-contact
10 μm
d)
λ (nm)
551 496 451 413 381 354 331 310 292 276
14 V
12 V
9.6 V
7 V
VB
GaN QWs
YB
EL intensity (a.u)
E (eV)

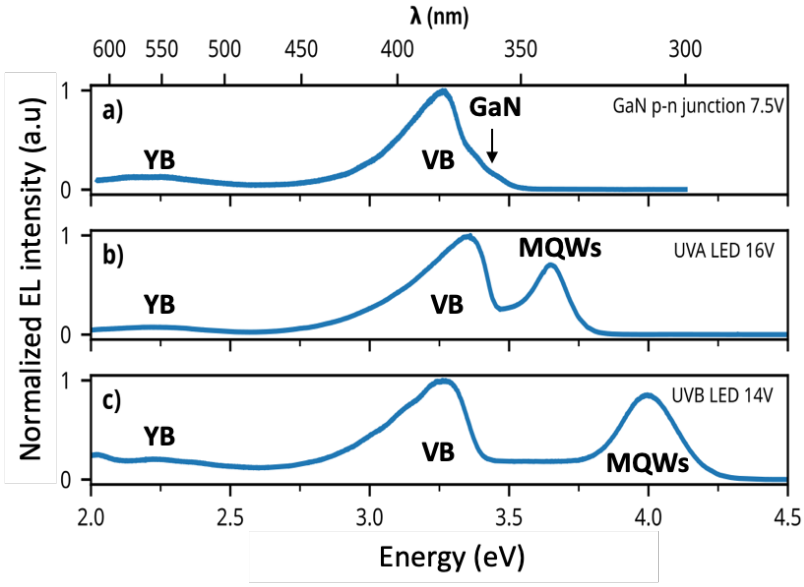
λ (nm)
600
550
500
450
400
350
300
Normalized EL intensity (a.u)
1
0
a)
GaN
GaN p-n junction 7.5V
YB
VB
b)
MQWs
UVA LED 16V
YB
VB
c)
UVB LED 14V
YB
VB
MQWs
2.0
2.5
3.0
3.5
4.0
4.5
Energy (eV)